fibers

MDPI

Article

Numerical Analysis of Dual-Wavelength Tungsten-Tellurite Fiber Raman Lasers with Controllable Mode Switching

Elena A. Anashkina * and Alexey V. Andrianov

A.V. Gaponov-Grekhov Institute of Applied Physics of the Russian Academy of Sciences, 46 Ulyanov Street, 603950 Nizhny Novgorod, Russia

* Correspondence: elena.anashkina@ipfran.ru

Abstract: Fiber laser sources in the spectral range near 1.7–1.8 μm are in highly demand for a lot of applications. We propose and theoretically investigate a dual-wavelength switchable Raman tungsten-tellurite fiber laser in the 1.7–1.8 μm range which can produce two stable modes at frequencies separated by ~7 THz with a pump at 1.55 μm. The Raman waves shifted by 19.8 THz (mode 1) and 27.5 THz (mode 2) from the pump frequency can be generated near two different maxima of the Raman gain spectrum (gain is higher at 19.8 THz and twice lower at 27.5 THz). We numerically simulate two-mode Raman lasing with allowance for energy transfer from the pump wave to modes 1 and 2, and from mode 1 to mode 2 due to inelastic Raman scattering. Diagrams of generation regimes depending on system parameters are constructed. We demonstrate controlled switching between two modes by changing the pump power. For the same intracavity losses for both Raman modes at relatively low pump powers, only mode 1 is generated. At medium pump power, generation occurs simultaneously in both modes. At relatively high pump power, only mode 2 is generated near the weaker maximum. This effect seems surprising, but a rigorous explanation with allowance for the nonlinear interaction between mode 1 and mode 2 is found. When losses for one of the modes change, switching of the generated regimes is also predicted.

Keywords: Raman fiber laser; Raman gain; dual-wavelength laser; tungsten-tellurite glass fiber; mode competition

Citation: Anashkina, E.A.; Andrianov, A.V. Numerical Analysis of Dual-Wavelength Tungsten-Tellurite Fiber Raman Lasers with Controllable Mode Switching. *Fibers* **2023**, *11*, 84. https://doi.org/10.3390/fib11100084

Academic Editor: Paulo Caldas

Received: 27 July 2023
Revised: 18 September 2023
Accepted: 28 September 2023
Published: 10 October 2023

1. Introduction

The spectral range near 1.7 μm has unique properties. There are absorption peaks of different bio-molecules in this range. Moreover, there are absorption peaks of O–H, C–O, N–O, and C–H bonds near 1.7 μm. At the same time, this range belongs to the valley between the absorption bands of water. For these reasons, 1.7 μm fiber laser sources find applications in bio-imaging and medical treatment [1–3], gas sensing [4], material processing [5], and so on. There are different ways to obtain laser waves in the 1.7 μm range based on optical fiber technologies, with certain advantages and disadvantages. For instance, these are Tm-doped fiber lasers and amplifiers [6,7], Bi-doped fiber lasers and amplifiers [8,9], light converters based on Raman soliton self-frequency shift in nonlinear fibers [10,11], and Raman lasers [12–14]. In contrast to population inversion lasers that generate in the wavelength bands corresponding to radiative transitions and require certain pump wavelengths, Raman lasers have no such restrictions. This can be highly promising for the development of widely tunable lasers (in the presence of tunable pump sources) [15]. The development of nonlinear fiber sources based on Raman-assisted effects has attracted increasing attention in recent years [16–18]. In addition to silica fibers, tellurite fibers seem to be prospective nonlinear media by virtue of a large Raman gain and a large Raman shift of tellurite glasses [19–22].

As a rule, in experimental and theoretical works devoted to continuous-wave (CW) tellurite fiber Raman lasers, fibers based on zinc-tellurite glasses are studied [19,23,24]. For zinc-tellurite glasses, the Raman gain spectrum has two main maxima located near 430

and 740 cm^{-1}, and the gain near the maximum at 740 cm^{-1} is approximately twice as high [19–21,25]. In this case, Raman lasing occurs near the peak at a frequency shifted by 740 cm^{-1} relative to the pump. Due to the large frequency shift, high Raman gain, sufficiently high damage threshold, and wide transparency band with a red border of ~5–5.5 μm, zinc-tellurite glasses are very promising for use in cascade Raman lasers, especially in the mid-IR range [23]. Such schemes were theoretically studied, for example, in [23,24], where only one Raman wave was considered in each order. In this case, the frequencies of Raman waves in successive cascades differ by ~22 THz (740 cm^{-1}). However, there are other known compositions of tellurite glasses for which, in contrast to zinc-tellurite glasses, the Raman response function contains three distinct maxima. For tungsten-tellurite glasses, the first maximum is also located at about 430 cm^{-1}, the second maximum at about 650–750 cm^{-1}, and the third maximum at about 920–940 cm^{-1} [20,22]. Thus, tungsten-tellurite glass Raman lasers are promising for generation of the Stokes waves shifted by large values of 20 THz and 27 THz (in the first cascade) from the pump frequency. For comparison, the Raman shift in the first cascade for silica and germanate glasses is ~13 THz [26,27], for $As_{40}S_{60}$ glasses it is ~10 THz [28], and for $As_{40}Se_{60}$ glasses it is ~7 THz [28].

The Raman response function of the considered tungsten-tellurite ($87.5TeO_2$–$12.5WO_3$) glass is shown in Figure 1 according to experimental data presented in [20]. However, depending on the exact composition of the glass (the content of TeO_2 and WO_3 and other oxides), the gain near the third maximum (near 27.5 THz) can be either lower [20] or higher [22] than the gain near the second maximum (near 19.8 THz). Such a complex form of the Raman response function can lead to complex and counterintuitive dynamics of Raman lasing with mode competition, especially if the second maximum is larger than the third one. More recently, photonic devices based on tungsten-tellurite glasses have made it possible to discover a new regime of dual-wavelength Raman generation with a frequency separation between waves of about 6–7 THz. The nontrivial dynamics of Raman waves in a spherical microresonator made of tungsten-tellurite glass was experimentally demonstrated and theoretically explained, taking into account the competition of nonlinearly coupled modes, leading to such dual-wavelength lasing at wavelengths of 1.73 μm and 1.8 μm with a pump at 1.55 μm [29].

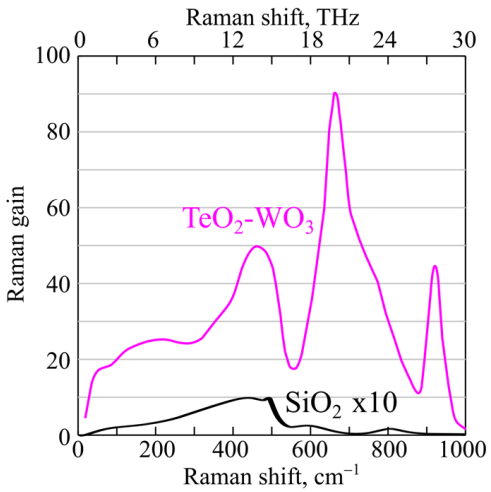

Figure 1. Raman gain spectra of TeO_2-WO_3 (magenta) and SiO_2 (black) glasses. Raman spectrum of SiO_2 glass is multiplied by 10.

In this work, we propose and theoretically investigate a CW multi-watt Raman fiber laser based on a tungsten-tellurite glass fiber which can generate two stable modes at frequencies separated by 7 THz. Such a laser may be of interest for many applications, including spectroscopy, remote sensing, medical treatment, the generation of terahertz radiation, and so on. We demonstrate controlled switching between two modes by changing the pump power. For the same intracavity losses for both Raman modes, at relatively

low pump powers, only the mode near the 2nd maximum of Raman gain (shifted by ~20 THz from pump frequency) is generated. At medium pump powers, generation occurs simultaneously in both modes near the 2nd (shifted by ~20 THz) and near the 3rd (shifted by ~28 THz) maxima. At relatively high pump powers, only the mode near the 3rd maximum (shifted by ~28 THz) is generated. The generation of a wave near the 3rd weaker maximum of the Raman gain in the absence of generation near the stronger 2nd maximum seems to be a surprising effect which, however, finds a rigorous explanation with allowance for the nonlinear interaction between these waves. When the losses for one of the modes change, switching between the generated regimes can also be observed. The study of dual-wavelength switchable generation in a tellurite fiber laser, in which both waves are located in the first cascade relative to the pump, was performed for the first time, although the experimental observation of non-laser multiple Raman peaks in a tellurite fiber was experimentally reported in [21]. CW Raman lasers based on tungsten-tellurite fibers have not been previously studied, to the best of our knowledge. The maximum Raman gain in tungsten-tellurite glasses is notably higher than that in zinc-tellurite glasses and is 2 orders of magnitude higher than that in silica and germanate glasses [20,22,27]. Thus, for TeO_2-WO_3(-Bi_2O_3) glass, Raman gain can be 80–120 times higher than the maximum value for silica glass [20,22]. Using a realistic design and experimental data from [20,29], we numerically demonstrate the prospects of using tungsten-tellurite fibers for CW multi-watt dual-wavelength switchable Raman lasers in the 1.7–1.8 μm range with a commercially available Er:fiber pump at 1.55 μm.

2. Materials and Methods

2.1. Conceptual Scheme

We have considered dual-wavelength Raman generation in tungsten-tellurite fiber lasers with a pump wave at 1550 nm that is readily achievable, for instance, using commercial or customized Er:fiber lasers. The developed model includes two Raman waves in the first cascade relative to the pump wave: mode 1 at 1727 nm and mode 2 at 1807 nm. These modes are down-shifted from the pump frequency by 19.8 THz and 27.5 THz, respectively, corresponding to the 2nd and 3rd maximums of the Raman gain spectra in Figure 1 [20]. Mode 1 and mode 2 are amplified by the pump; moreover, they nonlinearly interact with each other. Mode 1 amplifies mode 2 due to stimulated inelastic scattering with gain proportional to the Raman function at the difference frequency (27.5 THz–19.8 THz) = 6.7 THz. The mode interaction is illustrated schematically in Figure 2a.

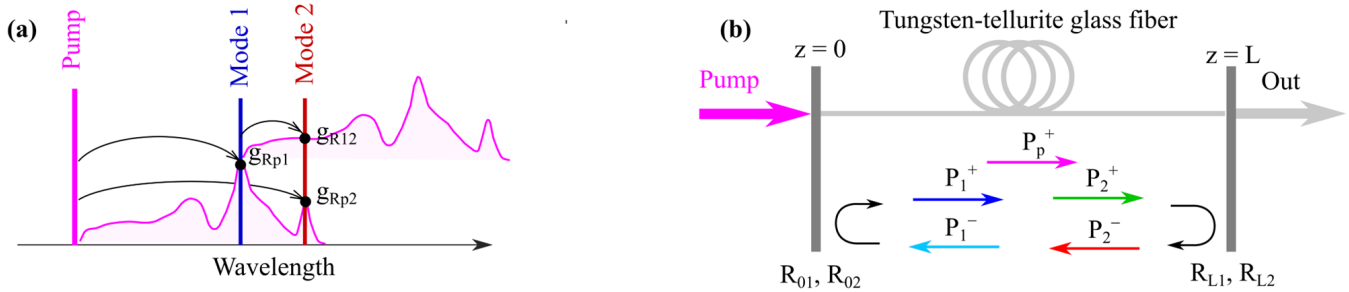

Figure 2. (**a**) Scheme of dual-wavelength Raman lasing taking into account Raman energy transfer: from 1550 nm pump to mode 1 at 1727 nm, from pump to mode 2 at 1807 nm, and from mode 1 to mode 2. g_{Rp1}, g_{Rp2}, and g_{R12} are Raman gain coefficients: for mode 1 amplified by pump wave, for mode 2 amplified by pump wave, and for mode 2 amplified by mode 1, respectively. (**b**) Scheme of dual-wavelength fiber Raman laser. P_p^+ is the power of forward-propagating pump wave; $P_{1,2}^+$ and $P_{1,2}^-$ are the powers in mode 1,2 propagating in forward and backward directions, respectively. $R_{01,02}$ and $R_{L1,L2}$ are the reflection coefficients for mode 1,2 at the input and output fiber ends, respectively.

We assumed that a laser resonator for mode 1 and mode 2 can be formed either by two pairs of Bragg gratings, or by mirrors, or reflective coatings applied to the fiber ends. The

specific implementation of the setup is not important here; only the reflection coefficients from each reflector are substantial. The adopted variant is shown in Figure 2b. The residual pump at the output fiber end did not return to the resonator.

2.2. Numerical Model

We analyzed fiber Raman lasers based on a tungsten-tellurite glass step-index fiber with core diameter d = 6 μm and numerical aperture NA = 0.18, providing single mode propagation for a pump wave at 1550 nm and Raman waves at 1727 and 1807 nm (with V-parameters being 2.189, 1.965, and 1.878, respectively). The effective mode field areas A_{eff} were calculated using the approximate analytical formula [26]:

$$A_{eff} = \frac{\pi d^2}{4}\left(0.65 + 1.619\mathrm{V}^{-\frac{3}{2}} + 2.879\mathrm{V}^{-6}\right)^2. \quad (1)$$

The set and calculated fiber parameters used in modeling are given in Table 1.

Table 1. Parameters of the fiber Raman laser used in modeling.

Parameter	Symbol	Value
Fiber core diameter	d	6 μm
Numerical aperture (core/cladding)	NA	0.18
Pump frequency (λ_p = 1550 nm)	f_p	193.5 THz
Frequency of mode 1 (λ_1 = 1727 nm)	f_1	173.75 THz
Frequency of mode 2 (λ_2 = 1807 nm)	f_2	166.0 THz
Effective area at λ_p = 1550 nm	A_{effp}	39 μm^2
Effective mode area at λ_1 = 1727 nm	A_{eff1}	47 μm^2
Effective mode area at λ_2 = 1807 nm	A_{eff2}	51 μm^2
Raman gain (for mode 1 amplified by pump wave)	g_{p1}	13.5×10^{-4} (W cm)$^{-1}$
Raman gain (for mode 2 amplified by pump wave)	g_{p2}	6.3×10^{-4} (W cm)$^{-1}$
Raman gain (for mode 2 amplified by mode 1)	g_{12}	2.8×10^{-4} (W cm)$^{-1}$
Fiber loss	α	0.3 dB/m (for Figures 3–5); 0…3 dB/m (only for Figure 6)
Reflection coefficient for mode 1,2 at z = 0	$R_{01,02}$	0.98
Reflection coefficient for mode 1,2 at z = L	$R_{L1,L2}$	0.05…0.95

The theoretical model describing cascade fiber Raman lasers of the nth-order with allowance for only one mode in each cascade is well known [30]. Here, it is of principal importance for us to take into account the Raman interaction between two modes in the first cascade generated near the 2nd and 3rd maxima of the Raman gain spectra near 19.8 THz and 27.5 THz, respectively (Figure 1). That is why we generalize the system of equations to include the Raman interaction between these nonlinearly coupled modes 1 and 2 according to the scheme in Figure 2a. We neglected cascade Raman lasing, for which the expected Raman wavelengths should be about 2 μm and beyond in the second cascade. We assumed that intracavity losses were high for second-cascade Raman waves since the reflection coefficients in the resonator were small at the corresponding wavelengths (which is easily achieved for Bragg gratings or selective dielectric mirrors). There was no modulation instability in the system since the considered fiber has normal dispersion and is not birefringent. Other possible four-wave mixing processes were also excluded. We checked that phase-matching conditions between possible sets of wavelengths were not met.

Thus, the master equations for the evolution of a pump wave with a power of $P_p{}^+(z)$ propagating in the forward direction and modes 1,2 propagating in both the forward and backward directions with powers $P_{1,2}{}^+(z)$ and $P_{1,2}{}^-(z)$, respectively, are written as [16,29,30]:

$$\frac{dP_p^+}{dz} = -g_{p1}\frac{f_p}{f_1}\left(P_1^+ + P_1^-\right)P_p^+ - g_{p2}\frac{f_p}{f_2}\left(P_2^+ + P_2^-\right)P_p^+ - \alpha P_p^+ \quad (2)$$

$$\pm\frac{dP_1^\pm}{dz} = g_{p1}P_p^+P_1^\pm - g_{12}\frac{f_1}{f_2}\left(P_2^+ + P_2^-\right)P_1^\pm - \alpha P_1^\pm \quad (3)$$

$$\pm\frac{dP_2^\pm}{dz} = g_{p2}P_p^+P_2^\pm + g_{12}\left(P_1^+ + P_1^-\right)P_2^\pm - \alpha P_2^\pm, \quad (4)$$

where α is the optical loss, g_{p1} (g_{p2}) is the Raman gain of mode 1 (mode 2) directly from the pump, and g_{12} is the Raman gain of mode 2 provided by mode 1 which depends on the Raman gain function at the difference frequency f_2–f_1. The Raman gain for the fiber is proportional to the Raman gain for the bulk glass (Figure 2a) inversely proportional to the amplifying wavelength, and inversely proportional to half sum of the areas of amplifying and amplified modes [26] (Table 1).

We assumed that the residual pump at the output end ($z = L$) was not recycled; hence, the boundary conditions were written only for mode 1 and mode 2 considering the reflection coefficients at the input (R_{01} and R_{02}) and output (R_{L1} and R_{L2}) ends:

$$P_1^+(0) = R_{01}P_1^-(0) \quad (5)$$

$$P_1^-(L) = R_{L1}P_1^+(L) \quad (6)$$

$$P_2^+(0) = R_{02}P_2^-(0) \quad (7)$$

$$P_2^-(L) = R_{L2}P_2^+(L). \quad (8)$$

To solve numerically the system of Equations (2)–(4) with the boundary conditions (5)–(8) we used the Runge–Kutta method adapted for such kind of problems [30].

3. Results

We have numerically simulated and investigated in detail CW dual-wavelength switchable Raman lasing in the framework of the developed two-mode model. An example of the evolution of pump power and intracavity powers of mode 1 at 1727 nm and mode 2 at 1807 nm for parameters of the system when two modes are generated simultaneously is presented in Figure 3.

First, we studied the features of dual-wavelength Raman lasing for various pump powers and output reflection coefficients for the fixed intracavity fiber length L = 1 m. A diagram of different generation regimes is displayed in Figure 4a. The horizontal green dash-dotted line in Figure 4a corresponds to $R_{L1} = R_{L2} = R_L = 0.45$. The output powers in mode 1 and mode 2 as a function of the pump power obtained by moving along this horizontal line are plotted in Figure 4b. The green pentagrams in Figure 4a,b show the interfaces between Raman generation regimes. At very low pump powers, the generation threshold is not reached for the Raman wave since the total losses exceed the gain. This case is labeled "I" in Figure 4a,b. With increasing pump power, the gain grows, and the generation threshold for mode 1 is first observed at the interface between areas I and II (assuming that the fiber losses and the losses on reflectors at $z = 0$ and $z = L$ are equal for mode 1 and mode 2). In area II, only Raman mode 1 is generated, and the total losses for this mode are compensated by the gain from the 1550 nm pump. As the pump is increased, the power of mode 1 at 1727 nm grows, and the gain for mode 2 at 1807 nm from the pump wave and from mode 1 also grows until it reaches total losses. The generation threshold for mode 2 is reached at the interface between areas II and III in Figure 4a,b. There is also area III in Figure 4a,b, where both modes coexist stably. In area III, the power of mode 1 decreases, whereas the power of mode 2 increases with increasing pump power. In this area,

the pump transfers its power due to stimulated Raman scattering to both waves at 1727 nm and at 1807 nm (according to Equations (2)–(4)); mode 1 also transfers power to mode 2 (according to Equations (3) and (4)). So, in area III, the total gain for each Raman mode exactly compensates for its losses. There is also a counterintuitive area of parameters IV in which only mode 2 is generated, although the Raman gain from the pump g_{p2} is less than g_{p1}. However, the explanation is that for mode 1, the total loss is determined not only by the fiber loss and losses on reflectors but also by losses due to stimulated Raman scattering into mode 2, which is seen from the term $-g_{12}(f_1/f_2)(P_2^+ + P_2^-)P_1^{\pm}$) in Equation (3). In area IV, the total losses for mode 1 are higher than the Raman gain from the pump. In area IV for mode 2, as for conventional (population inversion or Raman) single-color lasers, the higher the pump power, the higher the output laser power [31]. Thus, by changing the pump power at all other fixed parameters, one can control switching between the generated CW Raman waves at 1727 nm and 1807 nm, as well as obtain dual-wavelength Raman generation (Figure 4b).

We also investigated how the output reflectance affects the output Raman wave powers. It is well known from the general theory of lasers that there is an optimal value of the output reflection coefficient that provides maximum output laser power [31]. For our two-mode system, we obtained the same results. We set a pump power of 7.5 W and modeled the output powers in mode 1 and 2 as a function of the output reflection coefficients $R_{L1} = R_{L2} = R_L$ (Figure 4c), which corresponds to the motion along the vertical purple dash-dotted line in Figure 4a. Areas I, II, III, and IV are also shown in Figure 4c. In area IV, the maximum output power in mode 2 is obtained for $R_L{}^{opt} \sim 0.75$. In area IV, at $R_L > R_L{}^{opt}$, the intracavity power is high, but the fraction of outcoupled power is relatively small; at $R_L < R_L{}^{opt}$, the intracavity power is not high enough.

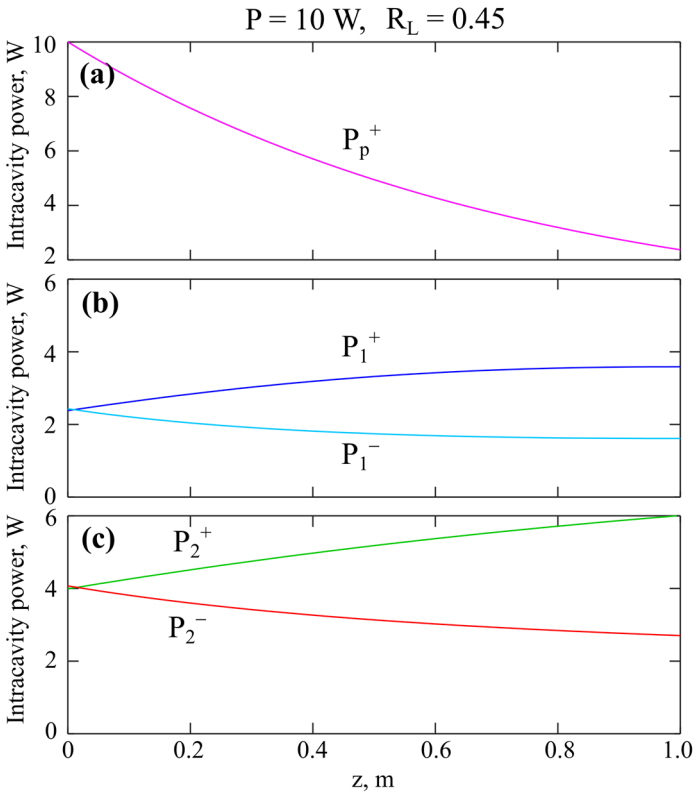

Figure 3. Evolution of intracavity powers of pump wave (**a**), mode 1 (**b**), and mode 2 (**c**) modeled for pump power of 10 W and reflection coefficients at the output $R_{L1} = R_{L2} = R_L = 0.45$.

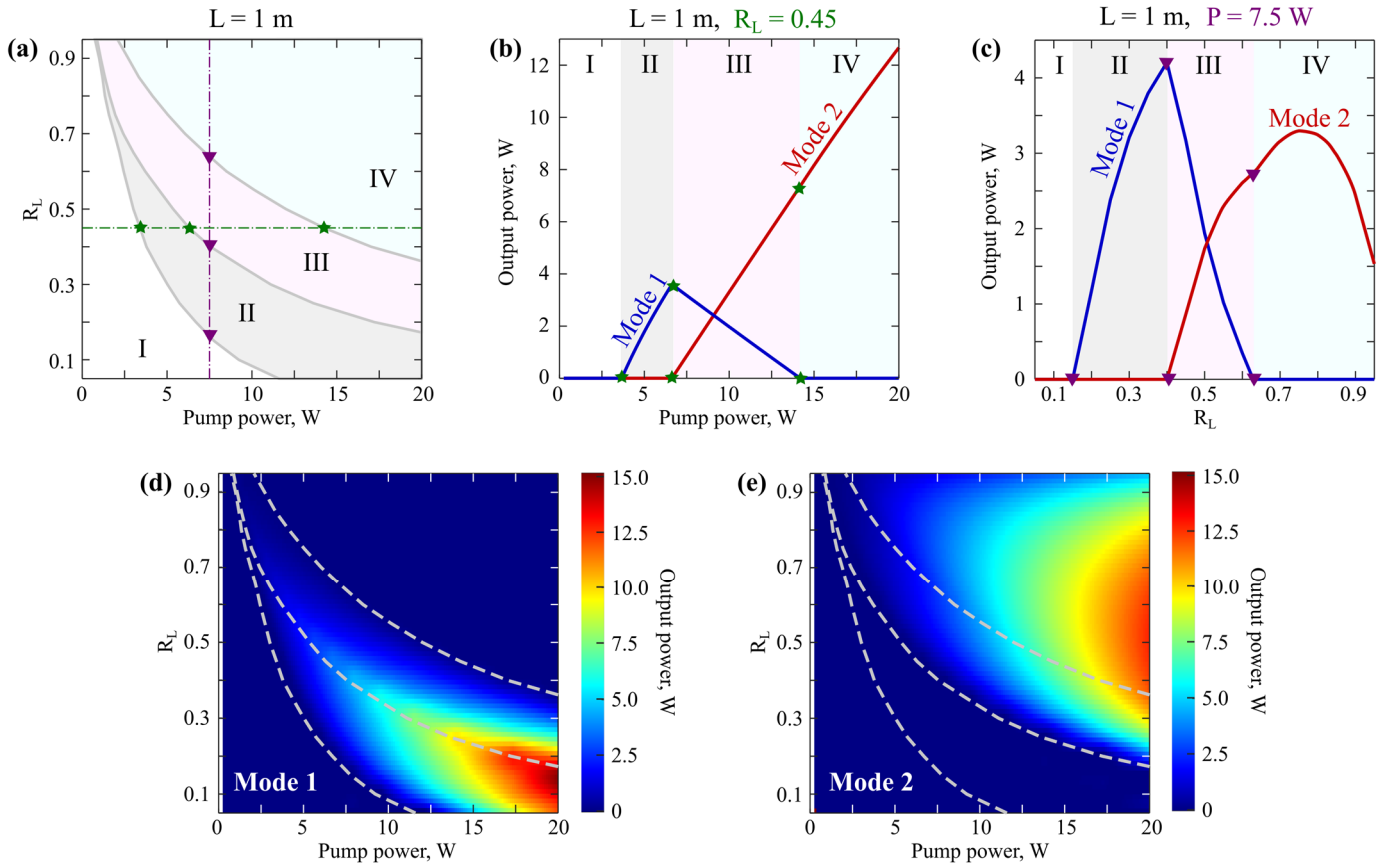

Figure 4. (**a**) Diagram demonstrating different CW regimes for varied pump power and output reflection coefficients $R_{L1} = R_{L2} = R_L$: no Raman generation (area I), Raman generation only in mode 1 (area II), Raman generation in mode 1 and mode 2 simultaneously (area III), and Raman generation only in mode 2 (area IV). (**b**) Output power of mode 1 and mode 2 as a function of pump power modeled for $R_{L1} = R_{L2} = R_L = 0.45$, corresponding to the green dash-dotted horizontal line in (**a**). (**c**) Output power of mode 1 and mode 2 as a function of output reflection coefficient $R_{L1} = R_{L2} = R_L$ modeled for pump power of 7.5 W, corresponding to the purple dash-dotted vertical line in (**a**). Output powers in mode 1 (**d**) and in mode 2 (**e**) depending on pump power and output reflection coefficients $R_{L1} = R_{L2} = R_L$. The dashed curves in (**d**) and (**e**) correspond to the interfaces of Raman regimes (**a**). All subplots were modeled for $L = 1$ m. The pentagrams in (**a**,**b**) and the triangles in (**a**,**c**) mark the interfaces between the regimes.

The output powers in mode 1 and mode 2 vs. pump power and output reflection coefficient are plotted in Figure 4d,e, respectively. The dash-dotted curves are the interfaces between different regimes, as shown in Figure 4a. The maximum output power in mode 1 is achieved at the interface between regimes II and III. The higher the pump power, the lower the optimal reflection coefficient for each mode. Figure 4d,e clearly demonstrate that low reflection coefficients (i.e., high intracavity losses) are favorable for the generation of mode 1 only, while high reflection coefficients (i.e., low intracavity losses) are favorable for the generation only of mode 2. For dual-wavelength or switchable Raman lasing, the reflection coefficient should be neither too low nor too high.

Next, we fixed the pump power at 10 W and simulated output powers in mode 1 and mode 2 as functions of intracavity fiber length and output reflection coefficients $R_{L1} = R_{L2} = R_L$. The diagram of Raman generation regimes for this pair of variables is given in Figure 5a. The meaning of areas I, II, III, and IV is the same as in Figure 4a. We plotted the output power in mode 1 (Figure 5b) and in mode 2 (Figure 5c) as a function of fiber length for selected values of output reflection coefficients of 0.1, 0.2, 0.4, 0.7, and 0.9, which are shown by dash-dotted horizontal lines in Figure 5a. For the considered

intracavity fiber lengths and small reflection coefficients, only mode 1 can be generated; mode 2 is below the threshold. For a representative example of $R_L = 0.1$, the horizontal line in Figure 5a intersects only areas I and II. The maximum power in mode 1 is reached at a certain length of about 2.7 m (Figure 5b). For $R_L = 0.2$, the dash-dotted line intersects three areas I, II, and III. Only mode 1 is observed in area II, and dual-wavelength lasing is observed in area III. For other selected examples, $R_L = 0.4$, 0.7, and 0.9, the dash-dotted lines intersect four areas: I, II, III, and IV. Thus, all regimes are realized, including lasing in mode 1 (area II), dual-wavelength lasing (area III), and lasing in mode 2 with complete suppression of mode 1 (area IV). When the horizontal line intersects at least three areas I, II, and III, the maximum output power in mode 1 is reached at the interface of areas II and III. Maximum output power in mode 2 can be reached at longer intracavity fiber lengths. The higher the reflection coefficient, the sharper the maxima for both modes.

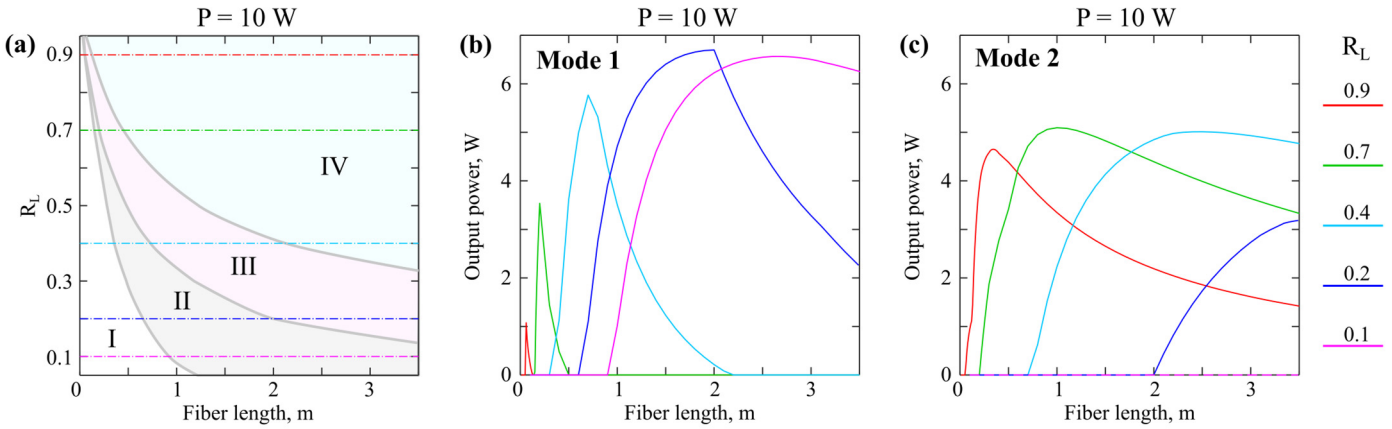

Figure 5. (**a**) Diagram demonstrating different steady-state regimes for varied intracavity fiber length and output reflection coefficients $R_{L1} = R_{L2} = R_L$: no Raman generation (area I), Raman generation only in mode 1 (area II), simultaneous Raman generation in mode 1 and mode 2 (area III), and Raman generation only in mode 2 (area IV). Output power of mode 1 (**b**) and mode 2 (**c**) as a function of intracavity fiber length for different output reflection coefficients $R_{L1} = R_{L2} = R_L$. All subplots were modeled for a pump power of 10 W.

Then, we studied how fiber optical loss affects the features of a dual-wavelength Raman laser. The diagram of Raman generation regimes as a function of pump power and fiber loss is plotted in Figure 6a for the intracavity fiber length $L = 1$ m and $R_{L1} = R_{L2} = R_L = 0.7$. The meaning of areas I, II, III, and IV is the same as in Figures 4a and 5a. We plotted the output power in mode 1 (Figure 6b) and in mode 2 (Figure 6c) as a function of pump power for selected values of fiber loss of 0.1, 0.3, 0.5, 1, and 2 dB/m, which are shown by dash-dotted horizontal lines in Figure 6a. The result that the higher the loss, the higher the threshold powers for each regime is quite expected. At high losses, the conditions for generating mode 1 are better, and at low losses, the conditions for generating mode 2 are better (Figure 6b,c). At first sight, it may seem counterintuitive that, with larger fiber losses, higher power can be achieved in mode 1. For example, the maximum out power is >2 W for a loss of 2 dB/m and <1 W for 0.3 dB/m. Meanwhile, the explanation is very simple: with increasing loss, the threshold for mode 2 becomes higher, and the maximum output power of mode 1 is reached at a higher pump power. Note that the slope efficiency of mode 1 (in area II) is lower for higher losses, which agrees with the general theory. For Raman lasing in mode 2, low fiber losses are preferable (Figure 6c).

Finally, we analyzed the case when output reflection coefficients are different for mode 1 and mode 2, which may be done using selective mirrors or Bragg gratings written for each wave. We fixed intracavity fiber length to be $L = 1$ m and $R_{L1} = 0.7$, while R_{L2} was varied. The output powers in mode 1 and mode 2 as a function of pump power are plotted in Figure 7a,b, respectively, for selected values, $R_{L2} = 0$, 0.1, 0.2, 0.4, 0.7, and 0.9. The higher

R_{L2}, the lower the threshold for mode 2. At the highest of the considered values $R_{L2} = 0.9$, mode 1 is not excited, and only mode 2 can be generated since total losses for mode 1 are higher than for mode 2 for any pump power. Thus, by varying the intracavity losses for mode 2, it is possible to control and switch the generation regimes.

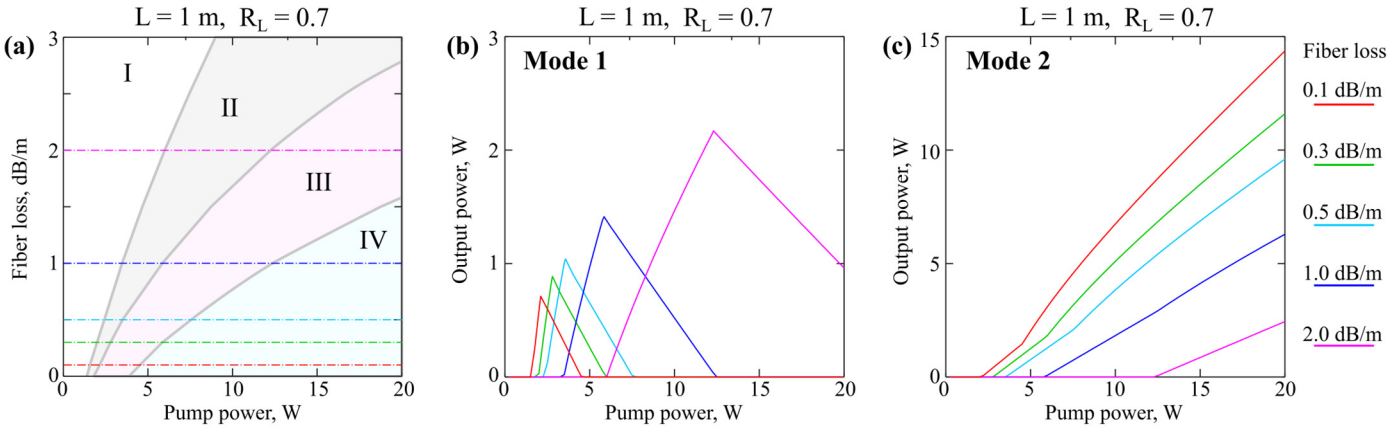

Figure 6. (**a**) Diagram demonstrating different steady-state regimes for varied pump power and fiber loss: no Raman generation (area I), Raman generation only in mode 1 (area II), Raman generation in mode 1 and mode 2 simultaneously (area III), and Raman generation only in mode 2 (area IV). Output power of mode 1 (**b**) and mode 2 (**c**) as a function of pump power modeled for different fiber losses. All subplots were modeled for $L = 1$ m and $R_{L1} = R_{L2} = R_L = 0.7$.

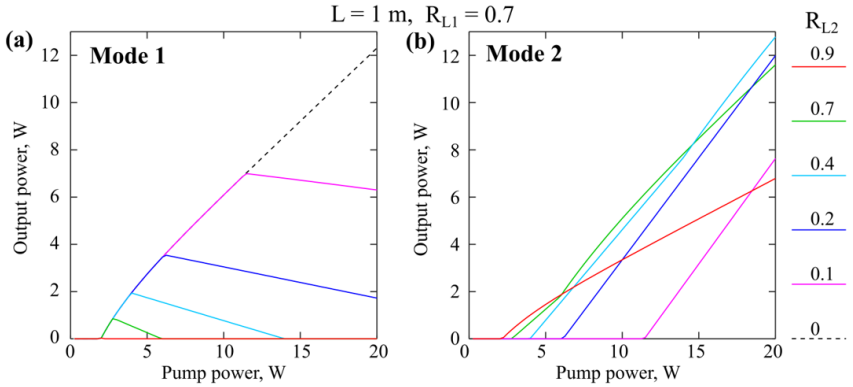

Figure 7. Output power of mode 1 (**a**) and mode 2 (**b**) as a function of pump power modeled for $L = 1$ m, $R_{L1} = 0.7$ and different values R_{L2}.

4. Discussion

We theoretically considered dual-wavelength Raman tungsten-tellurite glass fiber lasers with switchable modes operating in the 1.7–1.8 μm band with a pump wave at 1.55 μm with allowance for energy transfer between Raman modes. Note that Raman lasing with switching between modes 1 and 2 was previously experimentally observed in a tungsten-tellurite glass microresonator [29]. The results obtained here are in qualitative agreement with the experimental results of Ref. [29]. To the best of our knowledge, no experimental implementation of Raman lasing in tungsten-tellurite glass fibers has been reported yet.

The proposed idea and the developed theoretical model can be exploited for other operating wavelengths since diverse applications require laser sources in various spectral ranges. The developed approach can be easily used in the entire transparency window of tungsten-tellurite fibers. For instance, there is great interest in multi-watt laser sources at 1178 nm for further frequency doubling to produce yellow light at 589 nm [32]. Raman generation at 1178 nm can be obtained by operating with mode 2 (frequency-shifted from a 1.06 μm pump by 27.5 THz) using high-power Yb:silica fiber laser systems. Raman

lasers are also of particular interest at wavelengths > 2.2 μm, where laser sources are less developed than in the near-IR. For instance, with a pump at 2 μm available with Tm:silica fiber lasers, dual-wavelength Raman generation in a tungsten-tellurite fiber at ~2.3 μm and ~2.45 μm is expected. With a pump at 2.8 μm, available with Er:ZBLAN fiber lasers, Raman lasing at ~3.4 μm and ~3.8 μm is predicted. When developing Raman lasers outside the 1.7 μm spectral band considered in the work, the optimal parameters of a tungsten-tellurite fiber and the scheme will change, but it is easy to calculate them in the framework of the presented model.

5. Conclusions

To conclude, we proposed and theoretically studied a dual-wavelength switchable Raman tungsten-tellurite fiber laser which can produce two stable modes at frequencies separated by ~7 THz (at 1.73 and 1.8 μm with a pump at 1.55 μm). The Raman waves shifted by 19.8 THz (mode 1) and 27.5 THz (mode 2) from the pump frequency can be generated near two different maxima of the Raman gain spectrum (gain is higher at 19.8 THz and twice lower at 27.5 THz). We developed a numerical model based on generalized coupled equations for the evolution of powers of the pump wave and of modes 1, 2 with allowance for the energy transfer from the pump wave to modes 1, 2 and from mode 1 to mode 2 due to inelastic Raman scattering. We performed detailed numerical studies of dual-wavelength switchable Raman lasing with varied parameters of the systems and investigated specific features of the nonlinear behavior of the Raman waves. Diagrams of the generation regimes vs. system parameters were plotted. It was shown that by varying pump power, the following regimes may be implemented in the system: (I) no Raman lasing; (II) Raman lasing only in mode 1; (III) simultaneous Raman lasing in modes 1,2; and (IV) Raman lasing only in mode 2. We studied the influence of cavity fiber length, losses, and reflection coefficients and found the corresponding dependences.

Therefore, the presented results demonstrating surprising nonlinear dynamics of two-mode Raman lasing are interesting from a fundamental point of view and may be used as guidance for developing an experimental system in a wide spectral range corresponding to the transparency band of tungsten-tellurite glass.

Author Contributions: Conceptualization, E.A.A.; methodology, E.A.A.; software, E.A.A.; validation, E.A.A. and A.V.A.; formal analysis, E.A.A. and A.V.A.; investigation, E.A.A.; data curation, E.A.A.; writing—original draft preparation, E.A.A.; writing—review and editing, A.V.A.; visualization, E.A.A. All authors have read and agreed to the published version of the manuscript.

Funding: The work was supported by the Center of Excellence «Center of Photonics», funded by the Ministry of Science and Higher Education of the Russian Federation, contract No. 075-15-2022-316.

Data Availability Statement: Data underlying the results presented in this article may be obtained from the authors upon reasonable request.

Conflicts of Interest: The authors declare no conflict of interest.

References

1. Li, C.; Shi, J.; Gong, X.; Kong, C.; Luo, Z.; Song, L.; Wong, K.K.Y. 1.7 μm wavelength tunable gain-switched fiber laser and its application to spectroscopic photoacoustic imaging. *Opt. Lett.* **2018**, *43*, 5849–5852. [CrossRef] [PubMed]
2. Li, C.; Shi, J.; Wang, X.; Wang, B.; Gong, X.; Song, L.; Wong, K.K.-Y. High-energy all-fiber gain-switched thulium-doped fiber laser for volumetric photoacoustic imaging of lipids. *Photon Res.* **2020**, *8*, 160–164. [CrossRef]
3. Kawagoe, H.; Ishida, S.; Aramaki, M.; Sakakibara, Y.; Omoda, E.; Kataura, H.; Nishizawa, N. Development of a high power supercontinuum source in the 1.7 μm wavelength region for highly penetrative ultrahigh-resolution optical coherence tomography. *Biomed. Opt. Express* **2014**, *5*, 932–943. [CrossRef] [PubMed]
4. Chambers, P.; Austin, E.A.D.; Dakin, J.P. Theoretical Analysis of a Methane Gas Detection System, Using the Complementary Source Modulation Method of Correlation Spectroscopy. *Meas. Sci. Technol.* **2004**, *15*, 1629–1636. [CrossRef]
5. Sugioka, K.; Cheng, Y. Ultrafast lasers—Reliable tools for advanced materials processing. *Light Sci. Appl.* **2014**, *3*, e149. [CrossRef]
6. Zhang, J.; Fu, S.; Sheng, Q.; Zhang, L.; Shi, W.; Yao, J. Recent Progress on Power Scaling and Single-Frequency Operation of 1.7-μm Thulium-Doped Fiber Lasers. *Opt. Laser Technol.* **2023**, *158*, 108882. [CrossRef]

7. Szewczyk, O.; Łaszczych, Z.; Soboń, G. Spectral Compression and Amplification of Ultrashort Pulses Tunable in the 1650–1900 nm Wavelength Range. *Opt. Laser Technol.* **2023**, *164*, 109465. [CrossRef]
8. Firstov, S.V.; Alyshev, S.V.; Riumkin, K.E.; Melkumov, M.A.; Medvedkov, O.I.; Dianov, E.M. Watt-Level, Continuous-Wave Bismuth-Doped All-Fiber Laser Operating at 1.7 μm. *Opt. Lett.* **2015**, *40*, 4360–4363. [CrossRef]
9. Thipparapu, N.K.; Wang, Y.; Wang, S.; Umnikov, A.A.; Barua, P.; Sahu, J.K. Bi-doped fiber amplifiers and lasers [Invited]. *Opt. Mater. Express* **2019**, *9*, 2446–2465. [CrossRef]
10. Lee, J.H.; Howe, J.; Xu, C.; Liu, X. Soliton Self-Frequency Shift: Experimental Demonstrations and Applications. *IEEE J. Sel. Top. Quantum Electron.* **2008**, *14*, 713–723. [CrossRef]
11. Zolotovskii, I.O.; Korobko, D.A.; Okhotnikov, O.G.; Stolyarov, D.A.; Sysolyatin, A.A. Generation of a broad IR spectrum and N-soliton compression in a longitudinally inhomogeneous dispersion-shifted fibre. *Quantum Electron.* **2015**, *45*, 844–852. [CrossRef]
12. Zhang, Y.; Song, J.; Ye, J.; Xu, J.; Yao, T.; Zhou, P. Tunable Random Raman Fiber Laser at 1.7 μm Region with High Spectral Purity. *Opt. Express* **2019**, *27*, 28800–28807. [CrossRef]
13. Zheng, P.; Wu, D.; Dai, S. Wavelength Tunable Raman Fiber Laser Based on Raman Gain Spectrum Control. *Opt. Laser Technol.* **2023**, *164*, 109496. [CrossRef]
14. Pei, W.; Li, H.; Huang, W.; Wang, M.; Wang, Z. All-Fiber Tunable Pulsed 1.7 μm Fiber Lasers Based on Stimulated Raman Scattering of Hydrogen Molecules in Hollow-Core Fibers. *Molecules* **2021**, *26*, 4561. [CrossRef] [PubMed]
15. Andrianov, A.V.; Anashkina, E.A. Tunable Raman lasing in an As_2S_3 chalcogenide glass microsphere. *Opt. Express* **2021**, *29*, 5580–5587. [CrossRef] [PubMed]
16. Supradeepa, V.R.; Feng, Y.; Nicholson, J.W. Raman Fiber Lasers. *J. Opt.* **2017**, *19*, 023001. [CrossRef]
17. Kharenko, D.S.; Gervaziev, M.D.; Kuznetsov, A.G.; Podivilov, E.V.; Wabnitz, S.; Babin, S.A. Mode-Resolved Analysis of Pump and Stokes Beams in LD-Pumped GRIN Fiber Raman Lasers. *Opt. Lett.* **2022**, *47*, 1222–1225. [CrossRef]
18. Kuznetsov, A.G.; Nemov, I.N.; Wolf, A.A.; Evmenova, E.A.; Kablukov, S.I.; Babin, S.A. Cascaded Generation in Multimode Diode-Pumped Graded-Index Fiber Raman Lasers. *Photonics* **2021**, *8*, 447. [CrossRef]
19. Qin, G.; Liao, M.; Suzuki, T.; Mori, A.; Ohishi, Y. Widely Tunable Ring-Cavity Tellurite Fiber Raman Laser. *Opt. Lett.* **2008**, *33*, 2014–2016. [CrossRef]
20. Plotnichenko, V.G.; Sokolov, V.O.; Koltashev, V.V.; Dianov, E.M.; Grishin, I.A.; Churbanov, M.F. Raman Band Intensities of Tellurite Glasses. *Opt. Lett.* **2005**, *30*, 1156–1158. [CrossRef]
21. Cheng, T.; Gao, W.; Xue, X.; Suzuki, T.; Ohishi, Y. Experimental Investigation of Multiple Raman Peak Properties in a Hundred-Meter Tellurite Fiber. *Opt. Mater. Express* **2016**, *6*, 3438–3445. [CrossRef]
22. Okhrimchuk, A.G.; Yatsenko, Y.P.; Smayev, M.P.; Koltashev, V.V.; Dorofeev, V.V. Nonlinear Properties of the Depressed Cladding Single Mode TeO_2-WO_3-Bi_2O_3 Channel Waveguide Fabricated by Direct Laser Writing. *Opt. Mater. Express* **2018**, *8*, 3424–3437. [CrossRef]
23. Zhu, G.; Geng, L.; Zhu, X.; Li, L.; Chen, Q.; Norwood, R.A.; Manzur, T.; Peyghambarian, N. Towards Ten-Watt-Level 3–5 μm Raman Lasers Using Tellurite Fiber. *Opt. Express* **2015**, *23*, 7559–7573. [CrossRef]
24. Ni, C.; Gao, W.; Chen, X.; Chen, L.; Zhou, Y.; Zhang, W.; Hu, J.; Liao, M.; Suzuki, T.; Ohishi, Y. Theoretical Investigation on Mid-Infrared Cascaded Raman Fiber Laser Based on Tellurite Fiber. *Appl. Opt.* **2017**, *56*, 9171–9178. [CrossRef] [PubMed]
25. Sorokin, A.A.; Leuchs, G.; Corney, J.F.; Kalinin, N.A.; Anashkina, E.A.; Andrianov, A.V. Towards Quantum Noise Squeezing for 2-Micron Light with Tellurite and Chalcogenide Fibers with Large Kerr Nonlinearity. *Mathematics* **2022**, *10*, 3477. [CrossRef]
26. Agrawal, G.P. *Nonlinear Fiber Optics*, 6th ed.; Elsevier: Amsterdam, The Netherlands, 2019.
27. Dianov, E.M.; Mashinsky, V.M. Germania-Based Core Optical Fibers. *J. Light. Technol.* **2005**, *23*, 3500–3508. [CrossRef]
28. Li, W.; Seal, S.; Rivero, C.; Lopez, C.; Richardson, K.; Pope, A.; Schulte, A.; Myneni, S.; Jain, H.; Antoine, K.; et al. Role of S/Se Ratio in Chemical Bonding of As–S–Se Glasses Investigated by Raman, x-Ray Photoelectron, and Extended x-Ray Absorption Fine Structure Spectroscopies. *J. Appl. Phys.* **2005**, *98*, 053503. [CrossRef]
29. Anashkina, E.A.; Andrianov, A.V. Switchable Cascade Raman Lasing in a Tellurite Glass Microresonator. *ACS Photonics* **2023**, *10*, 1485–1494. [CrossRef]
30. Jackson, S.D.; Muir, P.H. Theory and Numerical Simulation of Nth-Order Cascaded Raman Fiber Lasers. *J. Opt. Soc. Am. B* **2001**, *18*, 1297–1306. [CrossRef]
31. Svelto, O.; Hanna, D.C. *Principles of Lasers*; Springer: New York, NY, USA, 2010.
32. Cai, Y.; Ding, J.; Bai, Z.; Qi, Y.; Wang, Y.; Lu, Z. Recent Progress in Yellow Laser: Principles, Status and Perspectives. *Opt. Laser Technol.* **2022**, *152*, 108113. [CrossRef]